Journées d'études: La Maîtrise du Frottement Sec, SBM 1990
17-18 octobre 1990 Bruxelles

EXPERIMENTAL AND NUMERICAL APPROACHES OF CONTACT WITH FRICTION AND WEAR IN LARGE DEFORMATION

S. CESCOTTO*, J. OUDIN**, R. CHARLIER*,
J.P. BRICOUT** and Y. RAVALARD**
*Département MSM, Université de Liège (Belgique)
** LGM Laboratoire de Génie Mécanique,
Unité Associée au CNRS 1401
MECAMAT, GRECO Calcul des Structures
Université de Valenciennes et du Hainaut Cambrésis (France)

SUMMARY

A review of main types of contact and friction between part and contactor and a set of isotropic and anisotropic surface constitutive equations are presented. Three typical tests are then described : upsetting of cylinders with bulk plastic deformation, indentation translation on parts specimens with localized plastic deformation, bench test of parts specimens until pickup. Examples show that realistic coefficients of surface constitutive equations are obtained with the simulation-scale tests and that practical data are directly enhanced.
Subsequently, the finite element modelling of contact-friction is exposed : implementation of a constitutive law of unilateral contact, of sticking and slipping friction conditions with a penalty method, development of a variational principle and of two functionals for the discretization of contact using mixed finite elements. Finally, three examples of finite element models with large strain, displacement and rotation are given : two dimensional models with loading of a crank head and drop forging of a hub, three dimensional model with rail rolling.

Keywords : plastic flow, elasto-plasticity, elasto-visco-plasticity, sliding velocity, contact, friction, lubrication,wear, finite element, penalty method, mechanical joint, forging, rolling

NOTATION

A_T, A_C, A_U	restrictions of boundary surface A
b	seating length
B	interpolation functions derivatives
C^e	elastic constitutive tensor
d^A, d^B	normal penetrations between contactor and part
e	thickness of lubricant film
$\underline{e}_1, \underline{e}_2, \underline{e}_3$	local base vectors on contact surface
$\underline{E}_1, \underline{E}_2, \underline{E}_3$	global base vectors on contact surface
f_F	yield potential
g_F	flow potential
F	body force
F_t	tangential force
F_n	normal load
G^*	virutal power functional
H	hardness
k	shear isotropic yield stress
K	stiffness matrix
K_c	contact tangential constitutive tensor
K_p, K_t	contact penalty factors
m	isotropic sublayer friction coefficient
m_v	visco-plastic friction coefficient
N	interpolation fucntions
p	effective penetration of indenter
p'	seating width
P	contact interpolation functions
q	contact stress discretization parameter
s	deviatoric stress tensor
t	time
T	surface traction vector
u	displacement
U	nodal displacement
u_t	sliding displacement
V	volume of the part
W_c	contact strain energy
W^*_c	complementary contact strain energy
x	coordinate
β	characteristical friction stress
ε_c	contact strain vector
ϕ	isotropic friction coefficient
η	viscosity
Π_c, Π_c^*	functionals
σ_S	Cauchy stress tensor
σ_c	contact stress vector
σ_n	contact pressure

σ_0	yield stress
τ, τ_1, τ_2	friction stress components
ξ	isoparametric coordinate
$\dot{f}$	time derivative of f
M^T	transpose of matrix M
M^{-1}	inverse of matrix M

1. INTRODUCTION

Large deformation problems are frequent in the mechanical engineering field and most of them involve non standard boundary conditions due to unilateral contact and friction. The influence of these conditions in the analysis of the problems has been often remarked mainly in the particular field of metal forming in which the most severe and the most various conditions are found [1,2,3]. The contact-friction system is somewhat analogous to the material part system for which macro scale and micro scale analyses are both required to get pertinent information. The macro scale variables for the parts and workpieces are the material flow stress, the composition and temperature ; the micro scale variables are, for the part, rugosity, adsorbed film, reaction film, bulk parent structure and for the contactor, matrix constitution, hard phase particles. For mechanical design purposes, some different numerical models of unilateral contact-friction systems have been proposed, see for instance [4, 5, 6, 7, 8].
The first aim is to have significant surface constitutive equations to take into account the most effective macro scale and micro scale parameters, the second is to implement the constitutive equations into numerical models. Contact occurrences involve kinematic and sthenic macroscopic variables : sliding velocity, contact pressure and friction stress. Depending of contact interfaces, generally one of these variables is a leader for the friction-contact problem and it corresponds to a constitutive equation. The determination of the coefficients and characteristical values of the above equations is recommended with three simulation scale tests : upsetting, indentation-translation and bench tests.
The hereafter presented numerical model has been

implemented in a finite element code dedicated to the analysis of elasto-plastic and elasto-visco-plastic bodies under large strains, displacements and rotations, i. e. in a highly non-linear context. The solution is obtained in using an updated Lagrangian description and Newton Raphson equilibrium iterations. Therefore, the approach is different from the other proposed ones because it takes into account very large displacements of the so-called contactors and of the strained body first, it uses the finite element concept with integration of the virtual power at the Gaussian integration points (based on a mixed variational principle) second and third it solves the non-linearity step by step with Newton Raphson iterations together with other non-linearities.

2. CONTACT AND FRICTION ANALYSES

The non standard boundary contact and friction conditions are effective in the virtual power functional which is the integral form of the equilibrium condition for the current volume V of the part [9]

$$G^*(u,\eta) = \int_V \sigma \nabla^S \eta \, dV - \int_{A_T} T \eta \, dA - \int_{A_c} \sigma_c \eta \, dA. \qquad (1)$$

In this equation, σ_c represents the contact and friction stress vector on the apparent contact surface A_c, T the standard surface traction vector prescribed on boundary surface A_c , σ the Cauchy stress tensor, η a virtual cinematically admissible field with $\eta = u$ on surface A_U and $\nabla^S\eta$ the symmetrised gradient of η.

2.1. BEHAVIOUR OF INTERFACES

The mechanical behaviour of interfaces is related to the properties of the part (workpiece), of the contactor (die) and of a third body which appears during the contact time or which has been deposited before contact. Microscopic observations show that the surface material of the part is not similar to the parent bulk material and typically, three main zones are

found : a 20-50 Ä adsorbed film, a 20-100 Ä oxide film and a 1-5 µm enriched-depleted layer (Fig. 1).

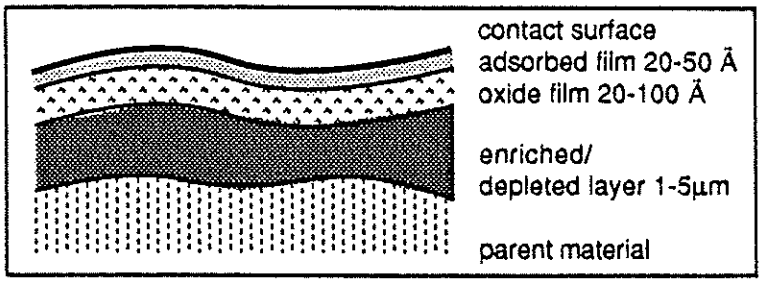

Fig. 1. Typical structure bounding contact surfaces.

Beside these local heterogeneities, the effective contact surface A_{ec} is more or less smaller than the apparent macroscopic one A_c due to the existence of surface asperities which profiles are various [10].

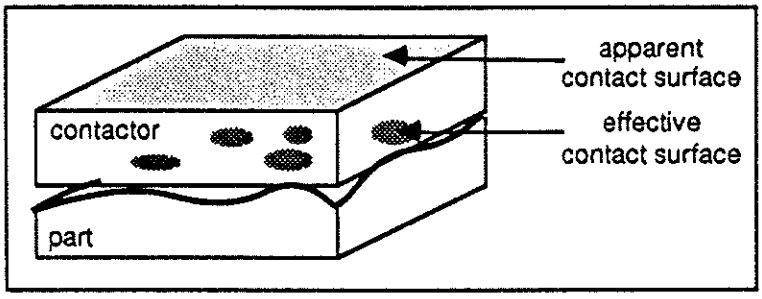

Fig. 2. Effective contact surface with a rough part.

A wider range of contact surface situations are obtained with deposited coatings, adhesives, lubricants depending on problems specifications. Six main situations are observed for most contacts : first, the dry contact with only two heterogeneous and rough surfaces, second, thick film lubricated contact in which the surfaces are separated by a lubricant the roughness being non influential [11] (Fig. 3a), third, thin lubricated contact in which the surfaces are also separated by a lubricant but the roughness is now influential (Fig. 3b) [12], fourth, boundary lubricated contact in which there are some asperities interactions (Fig. 3c), fifth, mixed lubricated contact which involves both thick film and boundary lubricated contact (Fig. 3d), sixth, solid film lubricated contact.

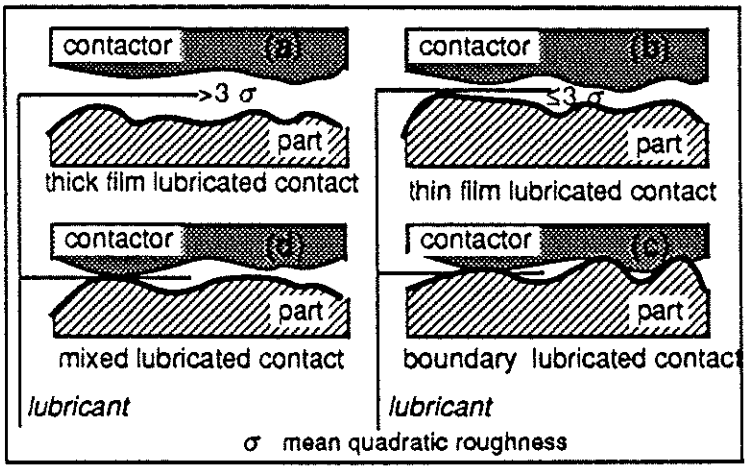

Fig. 3. Typical contact situations with deposited lubricant.

2.2. CONTACT AND FRICTION MODELS

The general model is a contact-friction function of two sets of parameters : first, material dependent parameters which include bulk and surface properties, impurities, coatings and lubricants properties ; strengthening dependent parameters which correspond to friction stress vector, contact pressure, sliding velocity, main plastic flow velocity, effective plastic strain, effective plastic strain rate and temperature. A first estimate of the friction force due to contact is

$F_t = A_{ec}\, m_c\, k$

with k the shear yield stress of the part (workpiece), m_c a coefficient equal to 1 for cleaned dry surfaces and lower than 1 for others (Fig. 5).

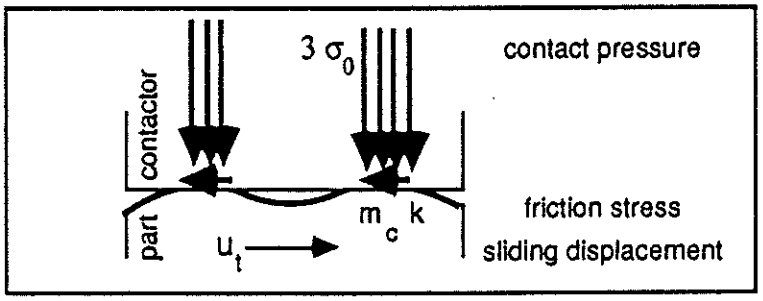

Fig. 5. Local contact friction stress at the top of surface asperities.

The pressure force is

$F_n = A_{ec}\, H \approx 3\, m_c\, A_{ec}\, \sigma_0$

with H the hardness of the part, and σ_0 the yield stress. The ratio between friction force and pressure

force is a global friction coefficient given by

$$\mu_G = \frac{F_t}{F_n} \leq \frac{1}{6} \qquad (2)$$

with $k = \sigma_0/2$

Let σ_n the contact pressure and τ the friction stress which are respectively the normal and tangent components of σ_c contact stress vector, u_t the relative tangential displacement of the part at contact occurrence. The local formulation which derives directly from relation (2) is the first order Coulomb's one

$$\tau = -\phi \, \|\sigma_n\| \frac{u_t}{\|u_t\|} \text{ with } \sigma_n \, n \leq 0 \qquad (3)$$

ϕ is a mean and isotropic friction coefficient which takes into account the non explicated parameters of the contact-friction situation. The local friction stress vector would not exceed the local yield stress, even if the contact pressure increases strongly ; so a more general expression is

$$\tau = -\text{Min}\{\phi(\|\sigma_n\| - \sigma^A), k\} \frac{u_t}{\|u_t\|} \qquad (4)$$

and in a second order form

$$\tau = -\text{Min}\{\phi_1(\|\sigma_n\| - \sigma^A) + \phi_2(\|\sigma_n\| - \sigma^A)^2, k\} \frac{u_t}{\|u_t\|} \qquad (5)$$

with σ^A the threshold normal stress (Fig. 6).

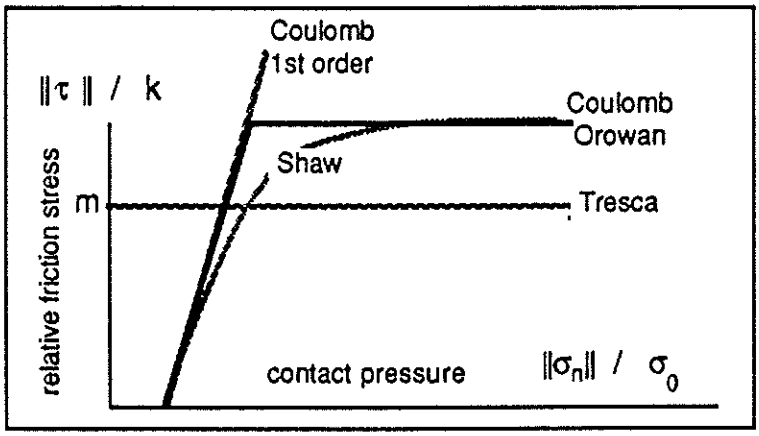

Fig. 6. Isotropic friction stress functions of contact pressure.

Considering now the effective contact surface instead of the contact pressure, the friction stress is ex-

pressed by the model of Shaw

$$\tau = - \alpha \; k \frac{u_t}{\|u_t\|} \tag{6}$$

α being the ratio A_{ac}/A_c. When the contact pressure is not very influential, the sublayer model function is used

$$\tau = - m \; k \frac{u_t}{\|u_t\|} \tag{7}$$

generalised by [13]

$$\tau = - m \; \frac{J_2}{\sqrt{3}} \frac{u_t}{\|u_t\|} \quad \text{with} \quad J_2 = \sqrt{\frac{3}{2} \mathbf{s} : \mathbf{s}}.$$

and **s** the deviatoric stress tensor. When considering now the surface roughness, the local friction stress is [14]

$$\tau_{local} = - m_{local} \; k \; \frac{u_t}{\|u_t\|}.$$

m_{local} is the local friction coefficient at the top of asperities. Then it becomes

$$\tau = - m_{local} \; \alpha \; k \; \frac{u_t}{\|u_t\|}. \tag{8}$$

Fig. 7 gives the form of the function (8) for a standard initial profile of asperities.

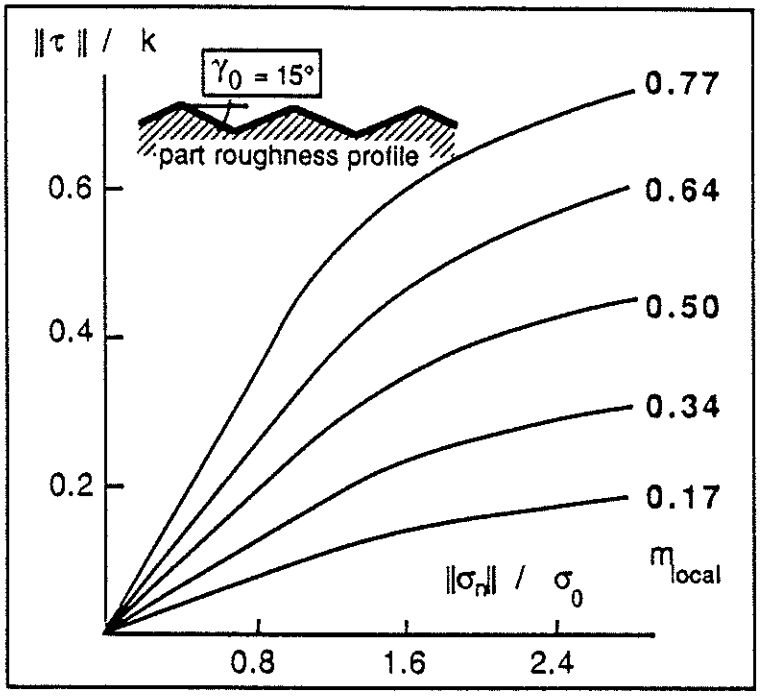

Fig. 7. Isotropic friction stress function of contact pressure with effective contact surface.

With thick film lubricating contact, the friction stress is given by

$$\tau = - \eta \; e \; \frac{u_t}{\|u_t\|} \qquad (9)$$

with e film thickness, η viscosity.
With a visco-plastic contact, the model is

$$\tau = - \beta \; \frac{\|v_t\|^{m_v}}{v_0^{m_v}} \frac{u_t}{\|u_t\|} \qquad (10)$$

in which β is the characteristical friction stress, v_t the sliding velocity, m_v the visco-plastic friction coefficient.
The above relations (3,4,5,6,7,8) become approximate for anisotropic behaviour, the sliding displacement vector direction is then different to the stress vector one. For instance, anisotropic formulation of equation (3) is

$$\sigma_c = - \sigma_n \, \mathbf{Q} \, \frac{u_t}{\|u_t\|}$$

with **Q** the friction tensor [15].

In most friction-contact occurrences, interactions between part (workpiece) and contactor (die) grow with contact time and so far, some supplementary wear-degradations of the surfaces are unavoidable. As for simple contact-friction situations, wear situations are various. Four main types can be presented : first, adhesive wear with local cold welding of asperities and generation of debris at the interface, second, abrasive wear with removal of material contactor by hard asperities or particles present into the candidate surfaces, third fatigue wear related to cyclic local stress and fourth chemical wear with material loss due to tribochemical reactions. The models are not at the moment as developed than those for contact-friction. However, it has been shown that the volume loss of material may be modelled by [16]

$$\Omega_w = K_u \frac{\|\sigma_n\|}{H} u_t$$

with K_u the mean adhesive-abrasive wear characteristic and H the hardness.

2.2. TYPICAL CONTACT-FRICTION TESTS

The aim of the tests is to determine realistic surface constitutive equations, related coefficients and characteristics. This means that strenghtening-dependent parameters are to be exactly defined. The secure approach would be full-scale tests but in most cases, measure devices are very expensive and on the other hand, the test analysis is limited to the particular case [17]. So, the more promising approach is to design a simulation scale test which is able to reproduce some of the most important strenghtening-dependent parameters values.
This is obtained with three tests which are effective for a large range of contact-friction problems : tests with bulk plastic deformation, test with localised plastic deformation, test with surface plastic deformation. During the tests, global measures, mainly loads, forces, displacements and eventually temperatures are the most effective.
Upsetting of cylinders is the typical simulation-scale test which involves bulk plastic deformation. The deformation of the cylinder depends on bulk constitutive equation and on surface one. So, from the measures of upsetting load, cylinder height and bar-

relling profiles, analyses of contact-friction between upsetting dies and cylinders are performed [18,19]. As example, Fig. 8 shows the evolution of the barrelling factor, the ratio between the equatorial diameter and the contact surface diameter, when isotropic elasto-plastic bulk constitutive equation and plastic isotropic surface constitutive equation from (7) is considered.

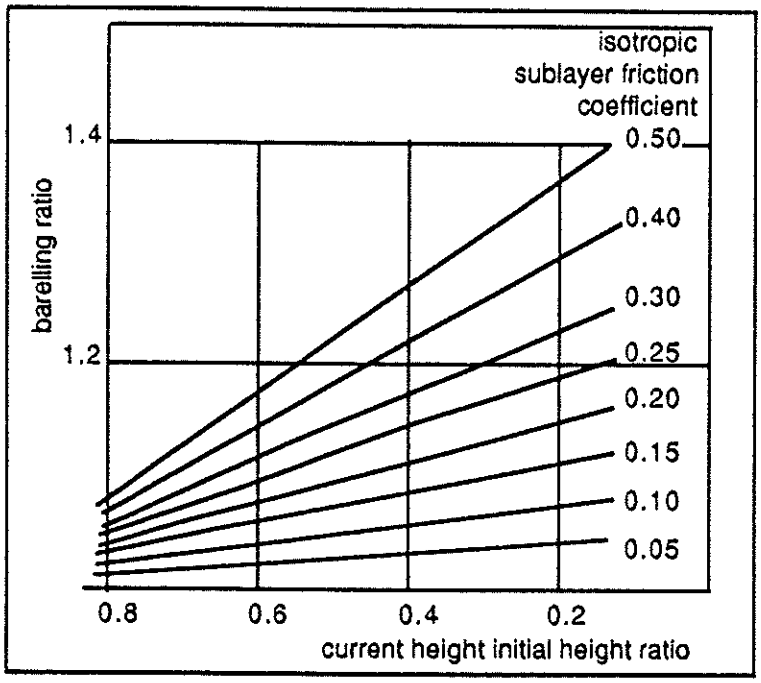

Fig. 8. Upsetting test of cylinders with 1.5 initial height- diameter ratio : abaque for determination of isotropic sublayer friction coefficient.

For the test achievement, it is essential to reproduce exactly the full scale contact-friction material-dependent parameters. For instance, the test has been used to find the isotropic sublayer coefficient at the extrusion punch top-workpiece interface. The upsetting dies were manufactured in the same conditions than punch ones : heat treated M44 steel, 64 HRC final hardness, 0.4 µm roughness. The specimen was a 10 mm diameter 15 mm height cylinder in a globularized 1018 steel on which a 4g.m^{-2} phosphate coating and stearate were deposited. From Fig. 8, the mean sublayer friction coefficient reaches 0.08 (extremums 0-0.16) when the bulk equivalent strain is 1.1, the equivalent strain rate 1 s^{-1}, the mean sliding velocity 0.25 mm.s^{-1} (extremums 0-0.5) and the mean sliding displacement 3 mm (extremums 0-6 mm).

In the indentation-translation test, localised plastic deformation is obtained by the translation of an indenter in the main tangential direction which corresponds to the local plastic flow direction in the full-scale problem (Fig. 9) [20]. The normal load and the tangential force are measured during the test. Fig. 10 gives an graph for the determination of the sublayer friction coefficient of equation (7).

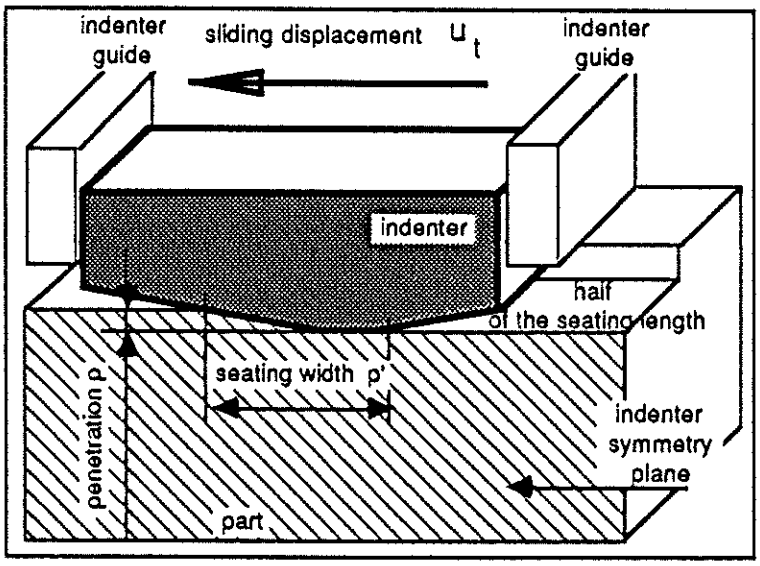

Fig. 9. Indentation-translation tests : experimental device.

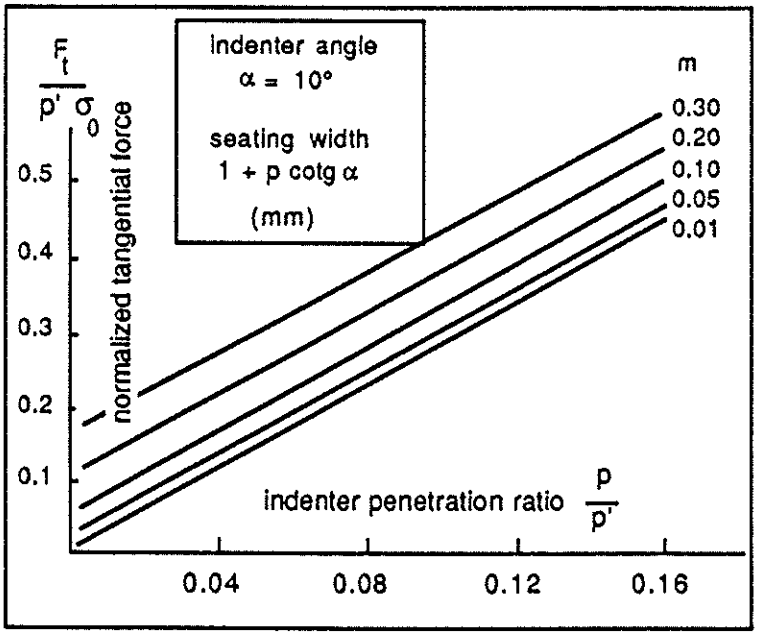

Fig. 10. Indentation-translation tests : graph for the determination of isotropic friction sublayer coefficients.

As example of the indentation-translation test, let choice the determination of the sublayer contact-friction coefficient during the cold drawing of heavy

1018 steel bars with heat treated D4 steel tools. Two sequences are involved in this problem. The dies roughness is 0.4 μm and phosphate stearate coatings are effective on the specimen surface (the specimen is here a portion of the full scale workpiece). With an indenter penetration of 0.35 mm which reproduces the essential process-dependent parameters during two successive indentations-translations, the sublayer contact-friction coefficient ranges from 0.09 in the first sequence to 0.17 in the second sequence, the sliding velocity being equal to 20 mm per second.

In the bench tests, light surface plastic deformation is achieved and mainly the third deposited body is influential here. In the device shown on Fig. 11, a small indenter presses on a cylindrical specimen which rotates as long as necessary to go to pickup [21]. The normal load is kept constant during the test and so, the friction tangential force is proportional to the result of local stress vectors. The global friction coefficient is given by relation (2).

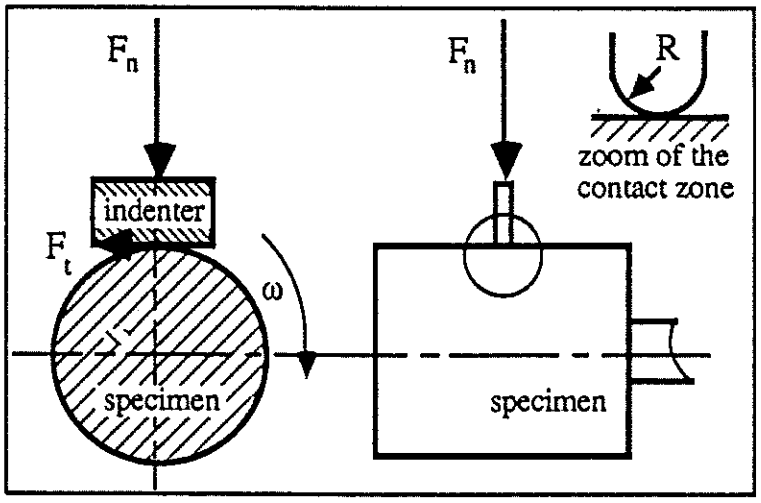

Fig. 11. Bench tests : experimental device.

Fig. 12 shows typical results for 1020 annealed steel ø60 mm cylindrical specimen with phosphate coating and stearate. The test gives the evolution of the global contact-friction coefficient during time contact. The coated surfaces deteriorate first slowly and then quickly at pickup occurrence.

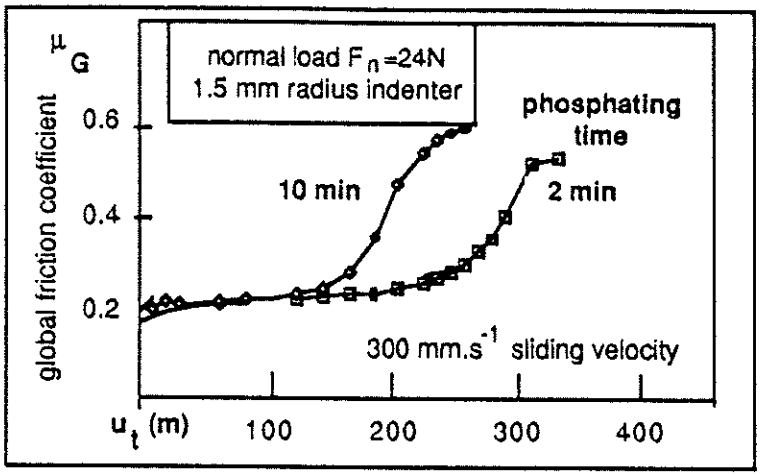

Fig. 12. Bench tests : global friction coefficient versus sliding displacement for two phosphating treatments.

3. NUMERICAL MODELLING OF CONTACT

Models of unilateral contact and friction problems have been achieved within the finite element framework of the LAGAMINE code developed in the MSM Department of the "Université de Liège" since 1982. This code is dedicated to the non linear analysis of large inelastic strains in solids. The bulk, elasto-plastic and elasto-visco-plastic, constitutive laws have an incremental form and the loading is done step by step.

3.1. MATHEMATICAL MODELS OF FRICTION LAW

The contact constitutive law is related to elasto-plastic formalisms proposed in [4, 22] and analysed in regard to thermodynamic principles in [23]. Let $\sigma_c=\{\sigma_n,\tau_1,\tau_2\}$ the contact stress vector and $\varepsilon_c=\{\varepsilon_n,\varepsilon_1,\varepsilon_2\}$ the contact strain. A gap (loss of contact) between contactor and part implies null contact stress $\sigma_c=\{0,0,0\}$. In the stress space, let consider a virtual elastic field bounded by a yield surface. Elasticity corresponds to sticking contact : real rigid and sticking contact occurrence is rather difficult to implement in a conventional finite element code and the elastic formulation is a penalised one for rigid and sticking contact. From a geometrical point of

view, elasticity of contact involves a small interpenetration of part and contactor. Thus, the contact elastic constitutive law is expressed by

$$\dot{\sigma}_c = \begin{bmatrix} K_p & 0 & 0 \\ 0 & K_t & 0 \\ 0 & 0 & K_t \end{bmatrix} \dot{\varepsilon}_c = C^e \dot{\varepsilon}_c$$

with K_p and K_t the contact penalty factors which are choosen as large as possible to limit interpenetration, the upper bounds depend on convergence degradation. Therefore, it is unrealistic to search any physical meaning for the above penalty factors.

For instance, the contact-friction yield surface related to equation (3) is expressed by

$$f_F = \sqrt{\tau_1^2 + \tau_2^2} - \phi \sigma_n$$

and other contact-friction yield surfaces are as easy to introduce in the finite element framework.
Irreversible contact strains correspond to the sliding displacements. In most mechanical problems, the normal irreversible displacement is rather weak, i.e. dilatancy equals almost zero. So, the associated flow rule applies as well but it is necessary to define a flow surface g_F such as

$$g_F = \tau_1^2 + \tau_2^2.$$

The contact strain rates are

$$\dot{\varepsilon}_c = \dot{\lambda} \frac{\partial g_F}{\partial \sigma_c}.$$

The last parameter to be defined is the hardening one which depends on the evolution of surface asperities, of the lubrication regime and of the wear occurrence. The lack of secure experiments leads to consider non hardening contact laws, that means

$$\dot{\phi} = 0 \quad \text{and} \quad \frac{\partial \phi}{\partial \dot{\lambda}} = 0.$$

The plasticity coefficient $\dot{\lambda}$ is obtained

from the consistency condition $\dot{f} = 0$

$$\dot{\lambda} = \frac{\frac{\partial f_F}{\partial \sigma_{c_j}} C^e_{ij} \dot{\varepsilon}_{c_{ij}}}{\frac{\partial f_F}{\partial \sigma_{c_a}} C^e_{ab} \frac{\partial g_F}{\partial \sigma_{c_b}}}$$

and the tangential constitutive tensor relating stress rates and strain rates is given by

$$\dot{\sigma}_{c_i} = K_c \dot{\varepsilon}_{c_j} = C^e_{ij} \dot{\varepsilon}_{c_{ij}} - \dot{\lambda} C^e_{ij} \frac{\partial g_F}{\partial \sigma_{c_j}}.$$

The above equations are time integrated.

The yield surface of two-dimensional and axisymmetric problems is represented in the stress space by a straight line and therefore the constitutive relation is linear either for elastic behaviour or for elasto-plastic one. The same integration scheme is convenient for both cases, the yield surface normal being unique. Three-dimensional problems involve a conical yield surface and a refined integration scheme is necessary : the time step is divided in some sub-increments in which a two-step generalised mid-point integration scheme is used [24, 25, 26].
The other important point is to ensure incremental objectivity when contact and part moves without deformation [27]. As shown in Fig. 13 with a constant velocity of the nodes, the normal contact strain is changing during the step.

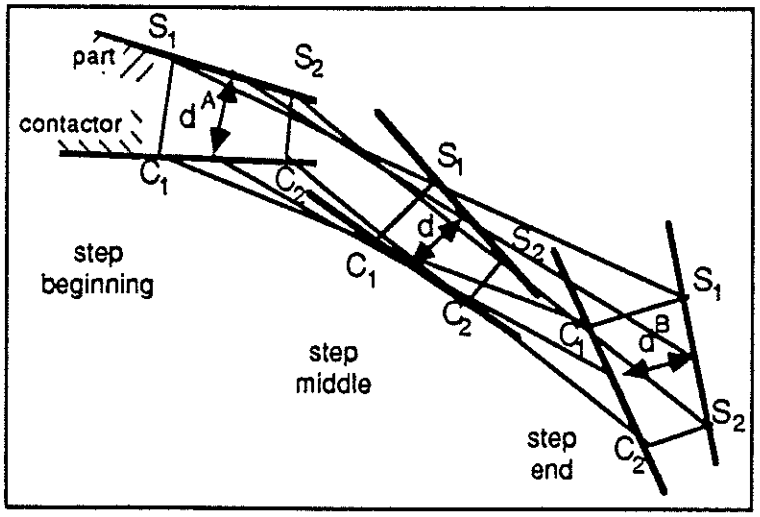

Fig. 13. Rigid motion of part and contactor during a time step : incremental objectivity analysis.

The objectivity is verified in changing the value of the

normal strain component as

$$\dot{\varepsilon}_1 = \frac{d_A - d_B}{dt}$$

with d_A, d_B, the penetration respectively at the beginning and the end of the time step dt.

3.2. FINITE ELEMENT DERIVATIONS

Modelling of unilateral contact involves special elements based on a mixed variational principle. Let consider first an isotropic and elastic part which takes the sticking contact with a high rigidity contactor.

Local coordinates at each geometric point of a smooth contact surface A_c are expressed in a $\underline{e}_1,\underline{e}_2,\underline{e}_3$ base vectors reference axis (Fig. 14). At a point S of surface A_c, σ_S is the Cauchy stress tensor in the part, σ_c the contact stress vector, u_S the part displacement vector and u_F the contactor displacement vector whose components are expressed in the local $\underline{e}_1,\underline{e}_2,\underline{e}_3$ reference axes :

$$\sigma_S^T = \{\sigma_{S_{11}}, \sigma_{S_{21}}, \sigma_{S_{31}}\} \; ; \; \sigma_c^T = \{\sigma_n, \tau_1, \tau_2\} \; ;$$

$$u_S^T = \{u_{S_{11}}, u_{S_{21}}, u_{S_{31}}\} \; ; \; u_F^T = \{u_{F_1}, u_{F_2}, u_{F_3}\} ;$$

and

$$\varepsilon_c = u_S - u_F .$$

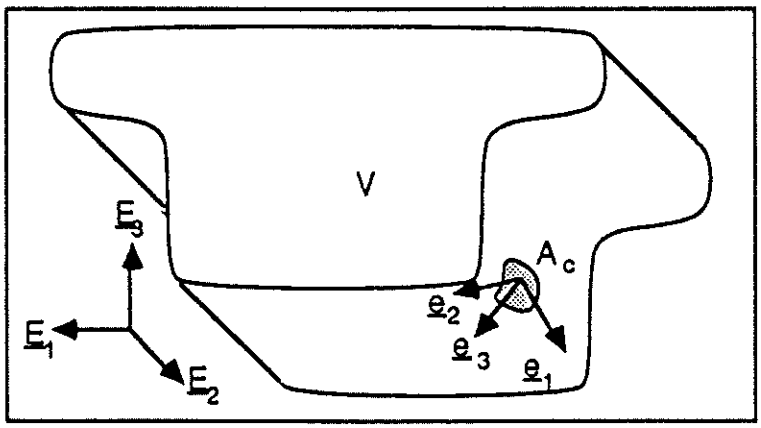

Fig. 14. Local base and global base vectors.

For points on surfaces A_U, A_T and in volume V, stresses σ, strains ε, displacements u, surface trac-

tion vectors T and body forces F are expressed in the global $\underline{E}_1, \underline{E}_2, \underline{E}_3$ reference axes :

$\sigma^T = \{\sigma_{11}, \sigma_{22}, \sigma_{33}, \sigma_{23}, \sigma_{13}, \sigma_{12}\}$

$\varepsilon^T = \{\varepsilon_{11}, \varepsilon_{22}, \varepsilon_{33}, 2\,\varepsilon_{23}, 2\,\varepsilon_{13}, 2\,\varepsilon_{12}\}$

$u^T = \{u_1, u_2, u_3\}$; $T^T = \{T_1, T_2, T_3\}$; $F^T = \{F_1, F_2, F_3\}$

$$\partial u^T = \left\{\frac{\partial u_1}{\partial X_1}, \frac{\partial u_2}{\partial X_2}, \ldots, \frac{\partial u_1}{\partial X_2} + \frac{\partial u_2}{\partial X_1}\right\}$$

$$\sigma_n^T = \{n_j\ \sigma_{j1}, n_j\ \sigma_{j2}, n_j\ \sigma_{j3}\}$$

$$\partial\sigma^T = \{\partial_j \sigma_{j1}, \partial_j \sigma_{j2}, \partial_j \sigma_{j3}\},$$

in which $\underline{n} = n_i\,\underline{E}_i$ is the outer normal to A_T or to A_U and $\partial_j = \partial/\partial X_j$.

Using the constitutive matrix K_c for sticking contact, the contact strain energy density W_c and the complementary energy W_c^* are given by

$$W_c(\varepsilon_c) = \frac{1}{2}\,\varepsilon_c^T\ K_c\ \varepsilon_c$$

$$W_c^*(\varepsilon_c) = \sigma_c^T\ \varepsilon_c - W_c = \frac{1}{2}\,\sigma_c^T K_c^{-1}\,\sigma_c.$$

Functionals Π_c^* and Π_c which differ in verifying or not the compatibility equation lead to the finite element discretization. Functional Π_c^* is expressed by

$$\Pi_c^* = \int_{A_c} \sigma_c^T [(u_S - u_F) - W_c^*]\, dA$$

$$+ \int_V [W(u) - F^T u]\, dV - \int_{A_T} T^T u\, dA \qquad (11)$$

where W(u) is the strain energy density in the part. The independent fields are u and σ_c since u_S is the restriction of u on A_c. The stationarity condition $\delta\Pi_c^*=0$ gives the compatibility equation

$$u_S = u_F = K_c^{-1}\,\sigma_c = \varepsilon_c \text{ on } A_c \qquad (12)$$

and the equilibrium equations are

$\sigma_c + \sigma_S = 0$ on A_c ; $\partial\sigma + F = 0$ on V ; $\sigma_n = T$ on A_T. (13)
For comparison with a more usual formulation, if the compatibility equation (12) is a priori satisfied, the following functional

$$\Pi_c = \int_{A_c} W_c \, dA + \int_V [W(u) - F^T u] \, dV - \int_{A_T} T^T u \, dA$$

is obtained in which the only independent field is u. The stationarity condition for Π_c gives the second equilibrium equation of set (12).
The stiffness matrix of two contact finite elements is computed from functionals Π_c^* and Π_c.
Compatible elements are used for the part volume discretisation and
$u = N U$; $\varepsilon = B U$
in which U are the nodal displacements, N the interpolation functions and B their derivatives.
The contact surface is discretized into finite elements the nodes of which coincide with those of underlying part elements. Hence, one has
$u_S = N_c U_c$
where U_c are the nodal displacements of the contact element and N_c
$N_c = A N$
is the restriction of N on A_c, A being a matrix the components of which are only 1 and 0. Finally the stress σ_c in the contact element is discretized by
$\sigma_c = P q$
where q are contact stress discretization parameters and P the corresponding interpolation functions.

Let

$$M_c = \int_{A_c} P^T N_c \, dA \; ; \quad X_c = \int_{A_c} P^T K_c^{-1} P \, dA$$

$$V_F = \int_{A_c} P^T u_F \, dA \; ; \quad K_S = \int_V B^T C B \, dV$$

$$F_S = \int_V N^T F \, dV + \int_{A_T} N^T T \, dA$$

$$k_c^* = M_c^T X_c^{-1} M_c \qquad f_c^* = M_c^T X_c^{-1} V_F$$

$$K = K_S + A^T k_c^* A \qquad F = F_S + A^T f_c^*$$

The discretized form of compatibility condition is
$M_c U_c - X_c q - V_F = 0$
from which the contact stress discretization parameters are computed

$$q = X_c^{-1} (M_c U_c - V_F) . \tag{14}$$

The discretized equilibrium equations are
$K U = F$.
It is seen that k_c^* is the stiffness matrix of the mixed contact element and f_c^* the corresponding nodal force vector.
For comparison, a compatible contact element derived from functional Π_c would have the following stiffness matrix and nodal force vector

$$k_c = \int_{A_c} N_c^T K_c N_c \, dA \; ; \; f_c = \int_{A_c} N_c^T K_c u_F \, dA.$$

Let consider a two-dimensional mixed element in which the displacement field is parabolic and the stress field linear (Fig. 15). Then

$$N = \begin{bmatrix} N_1 & 0 & N_2 & 0 & N_3 & 0 \\ 0 & N_1 & 0 & N_2 & 0 & N_3 \end{bmatrix},$$

$$P = \begin{bmatrix} P_1 & 0 & P_3 & 0 \\ 0 & P_1 & 0 & P_3 \end{bmatrix},$$

$$U^T = \{U_x^1\ U_y^1\ U_x^2\ U_y^2\ U_x^3\ U_y^3\},\ q^T = \{p_1\ \tau_1\ p_3\ \tau_3\},$$

$$N_1 = \frac{1}{2}\xi(1-\xi),\ N_2 = 1 - \xi^2,\ N_3 = \frac{1}{2}\xi(1+\xi),$$

$$P_1 = \frac{1}{2}(1-\xi),\ P_3 = \frac{1}{2}(1+\xi).$$

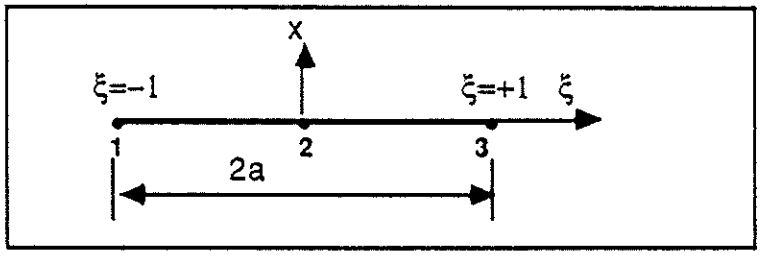

Fig. 15. Reference mixed contact element.

The calculation of k_c^* and f_c^* is straightforward and is omitted for conciseness. More interesting is the result deduced from (14) :

$$p_1 = K_p\left[\frac{1}{3}(2\,U_x^1 + 2\,U_x^2 - U_x^3) - u_{F_x}\right],$$

$$p_3 = K_p\left[\frac{1}{3}(2\,U_x^3 + 2\,U_x^2 - U_x^1) - u_{F_x}\right]. \qquad (15)$$

From this relation, it can be shown that that mixed element is equivalent to an underintegrated compatible element with parabolic displacement field developed from Π_c. For this objective, points ξ such that

$$p(\xi) = K_p\,[u_x(\xi) - u_{F_x}] \qquad (16)$$

with

$$p(\xi) = p_1 + P_1 + p_3\,P_3,$$

$$u_x(\xi) = U_x^1\ N_1 + U_x^2\ N_2 + U_x^3\ N_3$$

are searched. It is easily verified that relation (16) is satisfied for $\xi = \pm 1/\sqrt{3}$ which are the coordinates of the two Gauss points of the underintegrated parabolic element. Hence at these points, the contact pressure is exactly given by (15). This proves the equivalence of this mixed element with the underintegrated compatible parabolic contact element.

If the part is now submitted to large inelastic strains, the above developments are extended with the use of the corotational formulation. In the part, at each in-

tegration point, the Cauchy stresses are referred to a local frame rotating with the material particle.
On the contact surface, the local frame rotates with the corresponding surface element. In this frame, the incremental contact law with sliding and friction becomes non linear and non symmetrical

$$\dot{\sigma}_c = K_c \, \dot{\varepsilon}_c .$$

Hence, it can be shown that the following variational equation generalises the infinitesimal approach :

$$\int_V [\sigma^T \delta\varepsilon - F^T \delta u] \, dV - \int_{A_T} T^T \delta u \, dA$$

$$+ \int_{A_c} \sigma_c^T \delta u_S \, dA + \int_{A_c} [u_S - u_F - \varepsilon_c]^T \delta\sigma_c \, dA = 0 \qquad (17)$$

where

$$\varepsilon_c = \int_0^t K_{cT}^{-1} \dot{\sigma}_c \, dt, \quad u_S - u_F = \int_0^t [\dot{u}_S - \dot{u}_F] \, dt.$$

In (17) the integrals are taken over the current configuration of the part. The fact that the contact area A_c is a priori unknown is not a special problem because of the step by step solution in non linear analysis : at each step a simple search algorithm is used to determine the current contact area [28]. The development of mixed finite elements based on (17) closely follows the presented method and will not be detailed here. It is worth mentioning that one can also take advantage of the equivalence of underintegrated compatible elements in a context of large inelastic strains.

3.3. EXAMPLES

As first example, let consider a crank head composed of an aluminium tube deformed by a strong magnetic field to stick the steel insert (Fig. 16).

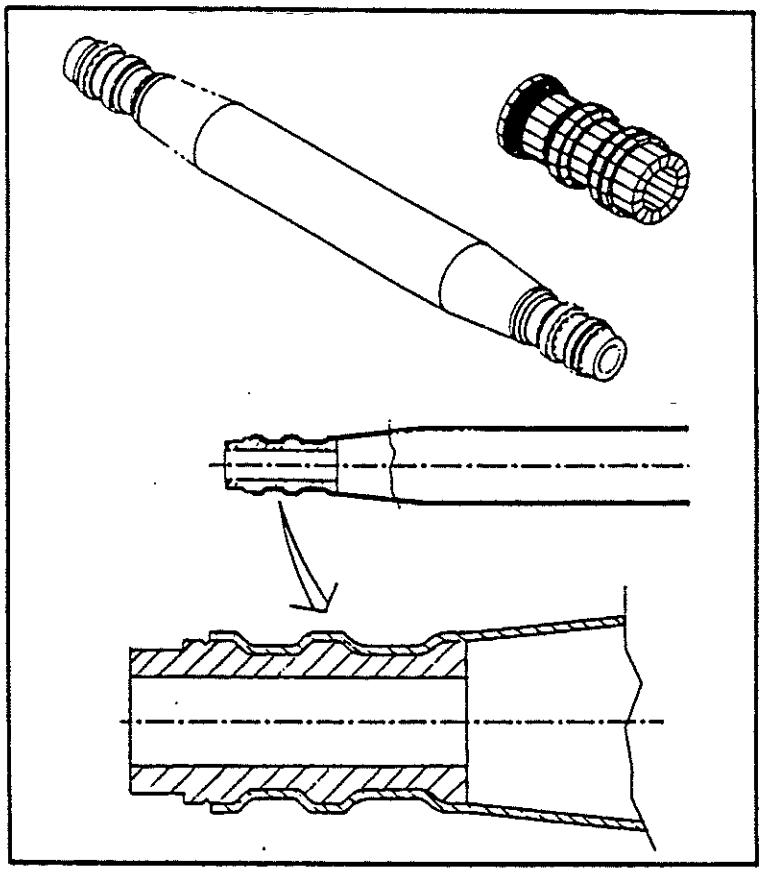

Fig. 16. Crank arm : general view, meridian cross section, zoom of the head zone.

The aim of the analysis is to predict the traction resistance of the head. Geometry and loading are axisymmetric, so that only the meridian cross section is modelled. The discretization consists in 54 axisymmetric eight nodes isoparametric elements. The aluminium constitutive law for the aluminium tube is elasto-plastic with isotropic hardening. In order to obtain prediction of the traction resistance on the safe side, friction coefficient ϕ was assumed to be zero. Fig. 17 shows the predicted evolution of the geometry of the tube near the steel insert. The tube convolutions are scaling progressively the insert humps.

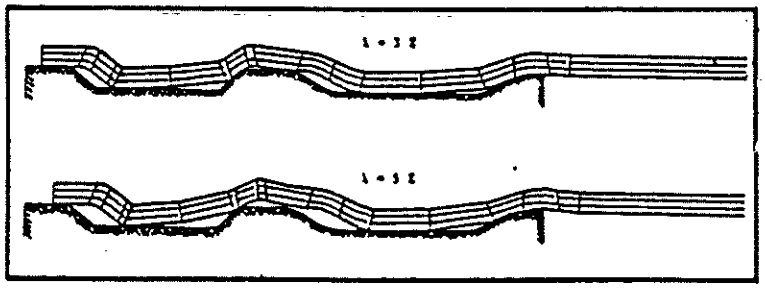

Fig. 17. Crank head finite element model, LAGAMINE code

computation : deformed mesh at 3 and 5% relative aluminium tube/steel insert displacement.

The computed values of the traction force versus axial displacement are presented on Fig. 18.

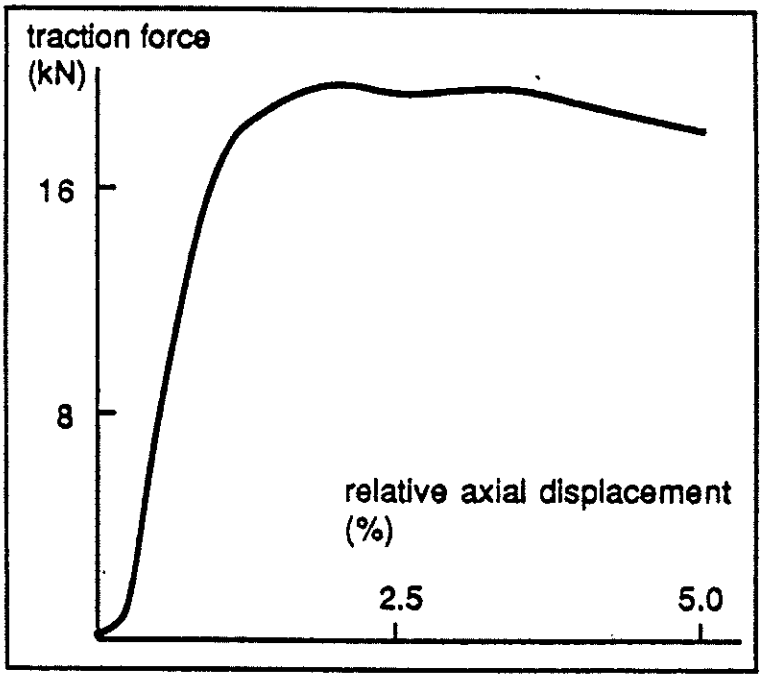

Fig. 18. Crank head traction resistance, LAGAMINE code computation : traction force versus relative displacement of the aluminium tube on the steel insert.

A second attractive example is the contact modelling of the drop-forging of a steel hub at 1150 °C The initial shape shape of the forged part (preform) and the contours of the rigid dies are given on Fig. 19.

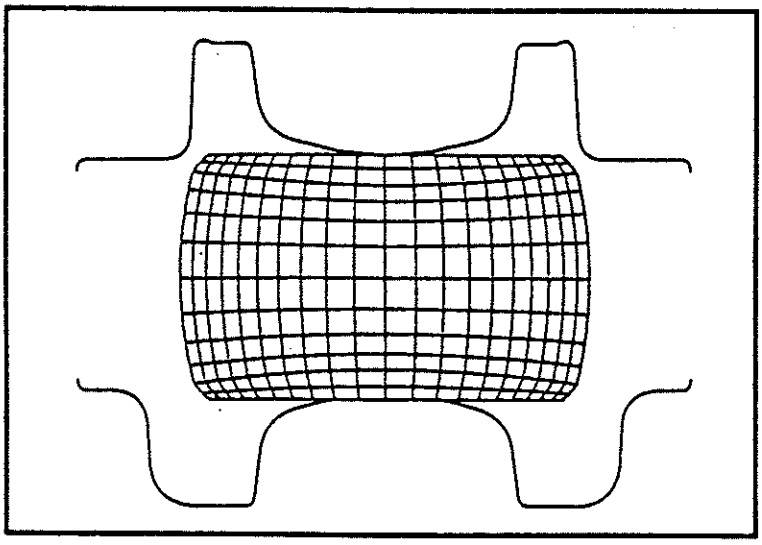

Fig. 19. Drop-forging of a steel hub, LAGAMINE code computation : initial finite element mesh.

High strain rates and large variations of the contact area are effective in this problem. A bulk elasto-visco-plastic constitutive equation and a surface Coulomb constitutive equation (3) are used. The friction coefficient ϕ is equal to 0.3.
Since the strains are very large, the initial finite element mesh is submitted to important distortions during the simulation so that it is necessary to perform four full remesh designs to obtain the final shape of the hub. The computed final shape of the hub and Von Mises equivalent stress distribution are shown on Fig. 20.

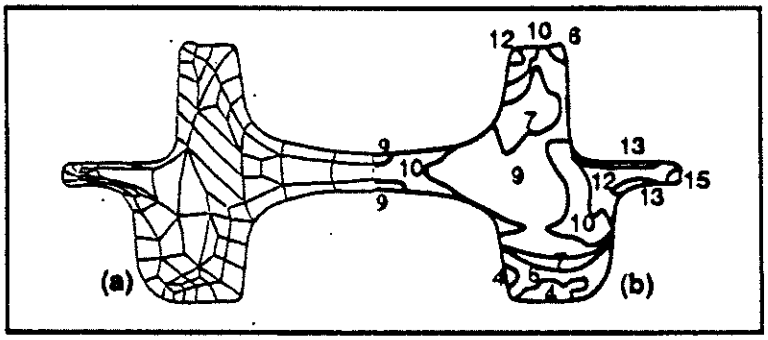

Fig. 20. Drop-forging of a steel hub, LAGAMINE code computation : (a) final state, (b) Von Mises equivalent stress.

The third example is the completely three-dimensional problem involved in rail rolling. In the case presented here the rail has no symmetry and it is modelled by 180 isoparametric elements (20 nodes solids, see Fig. 21).

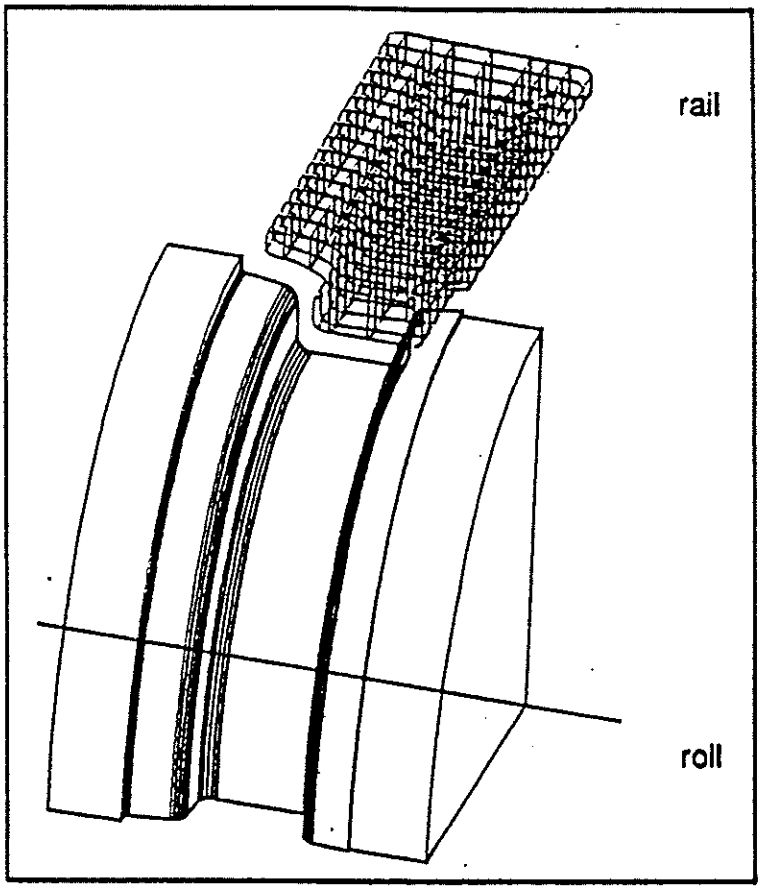

Fig. 21. Rail rolling : three-dimensional scheme of the problem.

The material is elasto-visco-plastic ; the parameters are determined according to rolling temperature and steel grade. The rolls are assumed to be rigid and the friction coefficient ϕ is equal to 0.3.The aim of the simulation was to determine the effect of a given rolling pass on a defect existing in the rail before the pass (Fig. 22). The final computed shape after the rolling pass shows that this defect is not eliminated (Fig. 23).

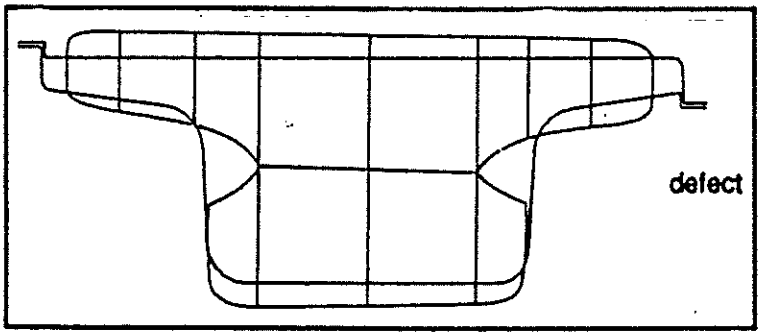

Fig. 22. Rail rolling : roll shape compared to the rollers before rollers processing.

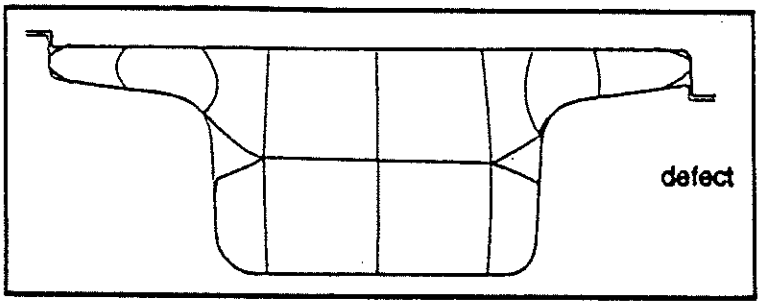

Fig. 23. Rail rolling, LAGAMINE code computation : rail after rollers processing.

CONCLUSION

The secure modelling of contact-friction and wear between contactors (dies) and parts (workpieces) is essential for mechanical problems analyses mainly in the case of large strain occurrences.
Typical interfaces without and with a third body are described : dry contacts, thick and thin film lubricated contacts, boundary lubricated contacts, mixed lubricated contacts and solid film lubricated contacts.
A set of contact-friction constitutive equations is then given in the form of friction stress vector function related to material and strengthening dependent parameters of the contact problem : effective contact surface, bulk yield stress, third body viscosity, contact pressure, sliding velocity.

Three typical simulation-scale tests, cylinder upsetting, indentation-translation and bench tests, are discussed for the determination of contact-friction equations and the related coefficients and characteristics. Practical results are given for isotropic plastic contact-friction equation in the form of graphes and typical values and curves.

Finite element modelling of unilateral contact with friction is then achieved in using a complete constitutive law for contact which includes unilateral conditions and sticking-sliding condition. A penalty approach is used and a typical application is given for the isotropic friction equation of Coulomb. Contact finite elements are based on a mixed variational principle for infinitesimal strain occurrences and then extended to inelastic large strain, large displacement and rotation problems. The formulation is shown to be equivalent to the cinematically admissible ele-

ment with Gauss underintegration.

Three typical finite element models are presented, axial loading of a crank head assembly, drop-forging of hubs and rail rolling, and the LAGAMINE code computations in the non linear finite element framework with unilateral contact and friction conditions are found to be quite efficient.

ACKNOWLEDGMENTS

The authors would like to thank "Ministère de l'Education et de la Recherche Scientifique de la Communauté Française", "Ministère de l'Education Nationale", the "Région Nord Pas de Calais", "CNRS", "Sous Commision des Echanges Scientifiques Belgique-France" for their support in the above developments.

BIBLIOGRAPHIE

[1] S. KALPAKJIAN, Recent progress in metal forming tribology, J. Applied Met. Work., 4, 3 (1986) 270.

[2] J.A. SCHEY, Tribology in metal working, friction, lubrication and wear, American Society for Metals, Ohio, 1983.

[3] K. LANGE, Handbook of Metal Forming, McGraw-Hill Book Company, 1985.

[4] A. CURNIER, A theory of friction, Int. J. Solids Struct., 20, N°7 (1984) 637.

[5] B. FREDRIKSSON, B. TORTENFELT and N. ENDAHL, Numerical solutions to contact, friction and crack problems with applications, Eng. Comp., Vol. 1 (1984) 133.

[6] J.T. ODEN and E. B. PIRES, Algorithms and numerical results for finite element approximations of contact problems with non classical friction laws, Comp. and Struct., Vol. 19, N°1-2 (1984) 137.

[7] J.C. SIMO, P. WRIGGERS and R.L. TAYLOR, A perturbed Lagrangian formulation for the finite element solution of contact problems, Comp. Meth. in Applied Mechanics and Engineering, N°50 (1985) 163.

[8] NGUYEN DANG HUNG and G. DE SAXCÉ, Frictionless contact of elastic bodies by the finite element methods and mathematical programming technique, Comp. and Struct., Vol. 11, N°1-2 (1980) 55.

[9] J. OUDIN, J.M. RIGAUT, J.C. GELIN and Y. RAVALARD, Approches expérimentales et numériques des conditions de contact et de frottement, Physique et Mécanique des Matériaux, F. MOUSSY et P. FRANCIOSI Eds., Presses du CNRS (1990) 406.

[10] J.T. ODEN and J.A.C. MARTINS, Models and computational methods for dynamic friction phenomena, Comp. Meths. Appl. Mech. Engng., 52 (1985) 527.

[11] T. B. LIM and D. H. SANSOME, Hydrodynamic lubrication in the tube-draw process, Tube International (March 1984) 34.

[12] W. R. D. WILSON, 1979, Friction and lubrication in bulk metal forming processes, J. Appl. Met. Work., 1, 1 (1979) 7.

[13] N. CRISTESCU, Plastic flow through conical converging dies using a constitutive viscoplastic equation, Int. J. Mech. Sci., 17 (1975) 425.

[14] N. BAY, Tool/workpiece interface stresses in cold forward extrusion, Adv. Techn. Plasticity, 1 (1984) 259.

[15] A. ZMITROWICZ, A theoretical model of anisotropic dry friction, Wear, 73 (1981) 9.

[16] P.H. HANSEN and N. BAY, Prediction of wear distribution in forming tools, Proceedings of the 9th International Conference on Experimental Mechanics, Lyngby, Copenhague (August 1990)

[17] B. LENGYEL and M. J. M. B. MARQUES, Friction along the fixed mandrel in the hydrostatic extrusion : drawing of tubes, Proceedings of the14th N.A.M.R.C. (1986) 394.

[18] J. C. GELIN, J. OUDIN and Y. RAVALARD, Determination of the flow stress-strain curves for metals from axisymmetric upsetting, J. Mech. Work. Techn., 5 (1981) 297.

[19] J. C. GELIN, J. OUDIN and Y. RAVALARD, Theoretical analysis and experimental applications of barelling and folding in cylinder upsetting tests, Int. J. Mech. Sci., 11, 12 (1984) 555.

[20] J.M. RIGAUT, J. OUDIN, J.P. BRICOUT, J. CABEZON and Y. RAVALARD, A new friction test procedure for the improvement of drawing and similar processes, J. of Mat. Proc. Technol., 3 (1990) 3-28.

[21] J.P. BRICOUT, J. CABEZON, J.M. RIGAUT, J. OUDIN et Y. RAVALARD, Approches expérimentales des conditions de contact, de frottement et de grippage en déformation à froid, Colloque Les Traitements de Surface avant Déformation à Froid, Association Française des Ingénieurs et Techniciens de l'Electrolyse et des Traitements de Surface A.F.T.S., F Paris (24-26 mai 1989) 121-137.

[22] A. CURNIER, Tact, a contact analysis program, Proc. of the 10th Leeds-Lyon Symposium on Development in Numerical and Experimental Methods applied in Tribology (1983).

[23] F. SIDOROFF, Etude thermodynamique des interfaces de frottement, Proceedings of Eurotrib' 85 (1985).

[24] J.R. RICE and D.M. TRACEY, Computational Fracture Mechanics, Proceedings of the Symp. on Num. and Comput. Meth. in Struct. Mech., S.J. FEVES, N. PERRONE, A.R. ROBINSON and SCHNOBRICK W.C. Eds., Academic Press (1973) 585.

[25] J.M.M.C. MARQUES, Stress computation in elasto-plasticity, Eng. Comp., Vol. 1 (1984) 42.

[26] R. CHARLIER, Approche unifiée de quelques problèmes non linéaires de mécanique des milieux continus par la méthode des éléments finis, Thèse de Doctorat, Département MSM, Université de Liège (1987).

[27] R. CHARLIER et S. CESCOTTO, Modélisation du phénomène de contact unilatéral avec frottement dans un contexte de grandes déformations, Journal of Theoretical and Applied Mechanics, Special isuues, Suppl. N° 1 to Vol. 7 (1988) 177.

[28] S. CESCOTTO, Computer aided methods for improved accuracy of drop-forging tools, BRITE project N° RI1B-0281-C(AM), research report N°2 (December 1989).